

Binding Potentials and Interaction Gates between Microwave-Dressed Rydberg Atoms

David Petrosyan^{1,2} and Klaus Mølmer³

¹*Aarhus Institute of Advanced Studies, Aarhus University, DK-8000 Aarhus C, Denmark*
²*Institute of Electronic Structure and Laser, FORTH, GR-71110 Heraklion, Crete, Greece*
³*Department of Physics and Astronomy, Aarhus University, DK-8000 Aarhus C, Denmark*
 (Dated: August 22, 2018)

We demonstrate finite range binding potentials between pairs of Rydberg atoms interacting with each other via attractive and repulsive van der Waals potentials and driven by a microwave field. We show that, using destructive quantum interference to cancel single-atom Rydberg excitation, the Rydberg-dimer states can be selectively and coherently populated from the two-atom ground state. This can be used to realize a two-qubit interaction gate which is not susceptible to mechanical forces between the atoms and is therefore immune to motional decoherence.

PACS numbers: 32.80.Ee, 32.80.Rm, 32.80.Qk 03.67.Lx,

Atoms in high-lying Rydberg states exhibit many remarkable features, including long lifetimes and giant polarizability [1]. The resulting strong, long-range, resonant (Förster) and nonresonant (van der Waals) dipole-dipole interactions between the atoms can suppress multiple Rydberg excitations within a certain blockade distance [2, 3, 5, 6]. In combination with laser and microwave field manipulation of atomic states, these interactions form the basis for quantum information processing [6] with individual atoms [2, 6–9] and atomic ensembles [3, 6, 10]. Furthermore, cold atoms excited to Rydberg states represent a flexible platform to simulate [11] and study few-body [12–21] and many-body physics [22–39].

A paradigmatic interaction phenomenon is the formation of a bound pair of particles. An electron in a Rydberg orbit scattering off a ground-state atom can sustain a weakly bound molecule with permanent dipole moment [12, 13]. Macrodimers of two Rydberg atoms can form due to van der Waals (vdW) interactions in a static electric field [14, 15] or through mixing of orbital angular momentum states [16]. Another binding mechanism relies on the Stark-shifted dipole-dipole (DD) interactions which can support Rydberg dimers [17] and trimers [18].

Here we identify a new mechanism to obtain long-range binding potentials between Rydberg atoms. Our two-atom potential curves result from microwave field coupling between a pair of Rydberg states of each atom [19]. Atoms in these states interact with each other via repulsive and attractive vdW potentials, and via typically weaker DD exchange interaction on the allowed microwave transition. When the attractive vdW interaction is comparable to, or stronger than, the repulsive vdW (and DD) interaction, the microwave-dressed potential energy curves have pronounced wells located in the vicinity of crossings of the two-atom attractive and repulsive potentials, in the frame rotating with the microwave frequency. The microwave field, which is detuned from the transition resonance of a single atom, lifts the degeneracy and causes level anti-crossing in the two atom basis. We

note that the combination of resonant and non-resonant DD interactions between the Rydberg atoms can also result in a binding potential [17].

We next address the question of how to selectively populate these Rydberg-dimer states starting from the two-atom ground state. The strong microwave field induces a broad dark resonance [40] for the laser excitation of a single (non-interacting) atom. We show that within this electromagnetically induced transparency (EIT) [41] window, a smooth probe laser pulse populates only the two-atom Rydberg manifold. We then propose to employ such a Rydberg dimer state to realize the universal CPHASE quantum logic gate between a pair of qubits represented by atoms trapped at a suitable distance from each other. This is implemented by coherent excitation and de-excitation of the atoms with a probe pulse of effective area 2π . The quantum interference responsible for EIT prevents Rydberg excitation of a single atom, and only an appropriate two-atom state acquires a conditional phase π . Since during the gate operation we populate the two-atom Rydberg state at the bottom of a potential well, there is no mechanical force between the atoms and motional decoherence [21] is suppressed.

Consider a pair of atoms with the Rydberg states $|e\rangle$ and $|r\rangle$ coupled by a microwave field with Rabi frequency Ω and detuning Δ , see Fig. 1(a). In the frame rotating with the microwave field frequency, the interaction Hamiltonian for atom $j = 1, 2$ reads $\mathcal{V}^j = -\hbar\Delta\hat{\sigma}_{rr}^j - \hbar\Omega(\hat{\sigma}_{re}^j + \hat{\sigma}_{er}^j)$, where $\hat{\sigma}_{\alpha\beta}^j \equiv |\alpha_j\rangle\langle\beta_j|$ denote the atomic operators. Atoms in states $|e\rangle$ and $|r\rangle$ interact via the vdW potentials $\mathcal{W}_{ee} = \hbar\frac{C_6^{ee}}{R^6}\hat{\sigma}_{ee}^1 \otimes \hat{\sigma}_{ee}^2$ and $\mathcal{W}_{rr} = \hbar\frac{C_6^{rr}}{R^6}\hat{\sigma}_{rr}^1 \otimes \hat{\sigma}_{rr}^2$, where R is the interatomic distance and C_6^{ee} and C_6^{rr} are the corresponding vdW coefficients. There is also a resonant DD (exchange) interaction between the atoms $\mathcal{D}_{er} = \hbar\sum_{i\neq j}\frac{C_3^{er}}{R^3}\hat{\sigma}_{re}^i \otimes \hat{\sigma}_{er}^j$, and an effective vdW interaction $\mathcal{W}_{er} = \hbar\sum_{i\neq j}\frac{C_6^{er}}{R^6}\hat{\sigma}_{rr}^i \otimes \hat{\sigma}_{ee}^j$ which arises from nonresonant DD interaction with shifted Rydberg level(s) [42]. The total Hamiltonian for the pair of Rydberg atoms is $\mathcal{H}_{2\text{Ry}} = \mathcal{V}^1 + \mathcal{V}^2 + \mathcal{W}_{ee} + \mathcal{W}_{rr} +$

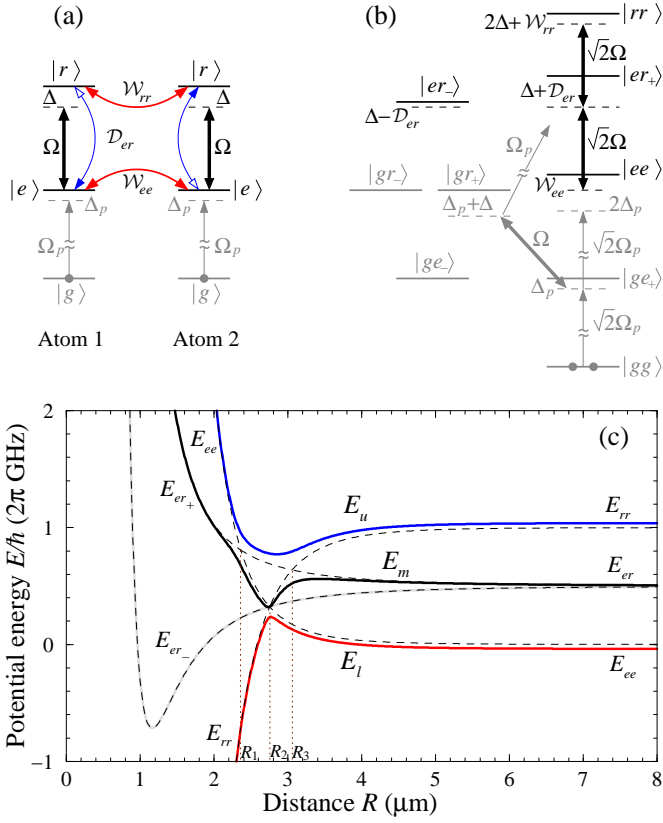


FIG. 1. (a) Atoms 1 and 2 with Rydberg states $|e\rangle$ and $|r\rangle$ interact via repulsive \mathcal{W}_{ee} and attractive \mathcal{W}_{rr} vdW interactions and DD (exchange) interaction \mathcal{D}_{er} , while a microwave field drives transition $|e\rangle \leftrightarrow |r\rangle$ with Rabi frequency Ω and detuning Δ . The Rydberg states can be excited from the ground state $|g\rangle$ by a probe laser field with Rabi frequency Ω_p and detuning Δ_p . (b) Diagram of levels and couplings in the two-atom basis. Antisymmetric states $|ge_{-}\rangle$, $|gr_{-}\rangle$ and $|er_{-}\rangle$ are decoupled from the laser and microwave fields. (c) Potential curves E_i , E_m , E_u for the two-atom microwave-dressed Rydberg states of Rb atoms with $|e\rangle \equiv |60S_{1/2}, m_j = +\frac{1}{2}\rangle$, $|r\rangle \equiv |60P_{3/2}, m_j = +\frac{3}{2}\rangle$, $\theta = \frac{\pi}{2}$, $\Omega = 2\pi \times 0.1$ GHz and $\Delta = -5\Omega$. Dashed curves correspond to bare ($\Omega \rightarrow 0$) energy levels E_{ee} , $E_{er_{\pm}}$, E_{rr} crossing at $R_{1,2,3}$.

$\mathcal{D}_{er} + \mathcal{W}_{er}$. Below we focus on the case of large detuning $|\Delta| \gg \Omega$, which exhibits rich structure and deep potential wells; the (near-)resonant case $|\Delta| \lesssim \Omega$ is discussed in [42].

Our two-atom basis set consists of states $|ee\rangle \equiv |e_1e_2\rangle$, $|er_{\pm}\rangle \equiv \frac{1}{\sqrt{2}}(|e_1r_2\rangle \pm |r_1e_2\rangle)$ and $|rr\rangle \equiv |r_1r_2\rangle$ [Fig. 1(b)]. When $\Omega \rightarrow 0$, the (bare) energies of states $|ee\rangle$ and $|rr\rangle$ are given by $E_{ee}/\hbar = C_6^{ee}/R^6$ and $E_{rr}/\hbar = -2\Delta + C_6^{rr}/R^6$, with $C_6^{ee} > 0$ (repulsive vdW interaction) and $C_6^{rr} < 0$ (attractive vdW interaction) while $\Delta < 0$ (red detuning). In turn, the resonant DD interaction lifts the degeneracy of states $|er_{\pm}\rangle$ whose energies are $E_{er_{\pm}}/\hbar = -\Delta \pm C_3^{er}/R^3 + C_6^{er}/R^6$, where $C_6^{er} > 0$ is due to the effective vdW interaction [42]. Figure 1(c) shows the dependence of bare energy levels $E_{\alpha\beta}$ on R . For vanishing

vdW and DD interactions, $R \rightarrow \infty$, $E_{ee} < E_{er_{\pm}} < E_{rr}$, while in the opposite limit of very strong (compared to $|\Delta|$) interactions, $R \rightarrow 0$, $E_{ee} > E_{er_{+}} > E_{er_{-}} > E_{rr}$ (in the rotating frame). There are three level crossing points of interest: $E_{ee} = E_{er_{+}} \equiv E_{c1}$ at R_1 , $E_{ee} = E_{rr} \equiv E_{c2}$ at R_2 , and $E_{rr} = E_{er_{+}} \equiv E_{c3}$ at R_3 , see [42].

Consider first the antisymmetric state $|er_{-}\rangle$. At large distance, the potential $E_{er_{-}} \propto -R^{-3}$ is attractive due to the long-range resonant DD interaction, but at smaller distances, the repulsive vdW interaction dominates, $E_{er_{-}} \propto R^{-6}$. Hence, $E_{er_{-}}$ has a potential well, $\partial_R E_{er_{-}} = 0$, around $R_{-} = \sqrt[3]{2C_6^{er}/C_3^{er}}$ where the vdW repulsion overcomes the DD attraction [Fig. 1(c)]. This simplified treatment captures the essential physics of the binding potential for DD interacting atoms presented in [17]. The antisymmetric state $|er_{-}\rangle$ will not play a role in our subsequent analysis since, for not too large dephasing, it is decoupled from the other two-atom states and the microwave field, even when $\Omega \neq 0$.

We are thus left with three basis states $|ee\rangle$, $|er_{+}\rangle$ and $|rr\rangle$ coupled sequentially by the microwave field with rate $\sqrt{2}\Omega$, see Fig. 1(b). At large distances $R > R_{2,3}$, the vdW (and DD) interactions are much weaker than $|\Delta|$ and the red-detuned ($\Delta < 0$) microwave field induces ac Stark shifts $\pm \frac{2|\Omega|^2}{\Delta}$ of levels $|ee\rangle$ and $|rr\rangle$ [Fig. 1(c)]. At small distances, $R < R_{1,2}$, the vdW and DD shifts are so large that levels $|ee\rangle$, $|rr\rangle$ and $|er_{+}\rangle$ decouple from the field. At the bare energy level crossing points R_1 and R_3 , the microwave field becomes resonant with the transitions $|er_{+}\rangle \leftrightarrow |ee\rangle$ and $|er_{+}\rangle \leftrightarrow |rr\rangle$. This leads to avoided crossings of the microwave-dressed energy levels E_u and E_m which are repelled from $E_{c1,c3}$ by $\pm\sqrt{2}\Omega$. The upper potential curve E_u has now a broad well near the crossing point R_3 of the bare levels $E_{er_{+}}$ and E_{rr} determined by the weakly repulsive DD interaction and strongly attractive vdW interaction. For the parameters used in Fig. 1(c), at the bottom of the potential well the vibration frequency of the two-atom relative motion is $\nu_u \simeq 2\pi \times 450$ kHz [42].

Similarly, at the bare level crossing point R_2 , the microwave field couples states $|ee\rangle \leftrightarrow |rr\rangle$, via nonresonant intermediate state $|er_{+}\rangle$, with the two-photon Rabi frequency $\Omega^{(2)} = \hbar \frac{|\sqrt{2}\Omega|^2}{E_{c2} - E_{er_{+}}(R_2)}$. Now the microwave-dressed energy levels E_l and E_m are repelled from E_{c2} by $\pm\Omega^{(2)}$, with the result that the middle potential curve E_m has a narrow well with a minimum near E_{c2} . With the above parameters, $\Omega^{(2)} = 2\pi \times 55$ MHz and the two-atom relative vibrational frequency in the vicinity of the potential well minimum R_m is $\nu_m \simeq 2\pi \times 2$ MHz [42]. Note that the interatomic potentials of Fig. 1(c) are azimuthally symmetric and robust with respect to small variations of the angle θ between the quantization axis and the two-atom separation vector, as shown in [42].

We next consider the excitation of the Rydberg states of atoms from the ground state $|g\rangle$ by a laser field acting

on transition $|g\rangle \rightarrow |e\rangle$ with the Rabi frequency Ω_p and detuning Δ_p , see Fig. 1(a). The total Hamiltonian for the pair of atoms is now $\mathcal{H} = \mathcal{H}_{2\text{Ry}} + \mathcal{V}_p^1 + \mathcal{V}_p^2$ with the interaction Hamiltonian $\mathcal{V}_p^j = \hbar\Delta_p\hat{\sigma}_{gg}^j - \hbar\Omega_p(\hat{\sigma}_{eg}^j + \hat{\sigma}_{ge}^j)$. We simulate the dynamics of the system using the master equation for its density operator $\hat{\rho}$, $\partial_t\hat{\rho} = -\frac{i}{\hbar}[\mathcal{H}, \hat{\rho}] + \mathcal{L}\hat{\rho}$, where the Liouvillian $\mathcal{L}\hat{\rho} = \sum_{j=1,2}(\mathcal{L}_g^j\hat{\rho} + \mathcal{L}_e^j\hat{\rho} + \mathcal{L}_r^j\hat{\rho})$, with $\mathcal{L}_\alpha^j\hat{\rho} = \frac{1}{2}[2\hat{L}_\alpha^j\hat{\rho}\hat{L}_\alpha^{j\dagger} - \{\hat{L}_\alpha^{j\dagger}\hat{L}_\alpha^j, \hat{\rho}\}]$, accounts for the relaxation processes affecting the atoms [43, 44]. These include the slow population decay of Rydberg states $|e\rangle, |r\rangle$ with rates $\Gamma_{e,r}$, and the usually more rapid decay of atomic coherences $\hat{\sigma}_{eg}$ and $\hat{\sigma}_{rg}$ with the total rate $\gamma = \gamma_g + \frac{1}{2}\Gamma_{e,r}$ ($\gamma_g \gg \Gamma_{e,r}$) which originates from the laser phase fluctuations, Doppler shifts due to thermal atomic motion, and intermediate state decay when $|g\rangle \rightarrow |e\rangle$ is a two-photon transition [6–8, 10, 38, 39]. The corresponding Lindblad generators are $\hat{L}_e^j = \sqrt{\Gamma_e}\hat{\sigma}_{ge}^j$, $\hat{L}_r^j = \sqrt{\Gamma_r}\hat{\sigma}_{gr}^j$ and $\hat{L}_g^j = \sqrt{\gamma_g/2}(\hat{\sigma}_{gg}^j - \hat{\sigma}_{ee}^j - \hat{\sigma}_{rr}^j)$.

We assume that a short probe laser pulse $\Omega_p(t)$ irradiates the pair of free (thermal) atoms, followed by the detection of atoms in the Rydberg states, e.g., through dc field ionization. We vary the probe field frequency Δ_p and interatomic distance R from pulse to pulse to obtain the Rydberg excitation probabilities shown in Fig. 2. The probabilities of a single $P_{1\text{Ry}} = \text{tr}(\hat{\rho}\hat{\Pi}_{1\text{Ry}})$ and double $P_{2\text{Ry}} = \text{tr}(\hat{\rho}\hat{\Pi}_{2\text{Ry}})$ excitations are defined through the projectors $\hat{\Pi}_{1\text{Ry}} \equiv \sum_{i \neq j}(\hat{\sigma}_{ee}^i + \hat{\sigma}_{rr}^i) \otimes \hat{\sigma}_{gg}^j$ and $\hat{\Pi}_{2\text{Ry}} \equiv (\hat{\sigma}_{ee}^1 + \hat{\sigma}_{rr}^1) \otimes (\hat{\sigma}_{ee}^2 + \hat{\sigma}_{rr}^2)$, where $\hat{\sigma}_{gg}^j + \hat{\sigma}_{ee}^j + \hat{\sigma}_{rr}^j = \mathbf{1}_j$; an actual experiment may or may not resolve the Rydberg state and atom (or ion) number, therefore both $P_{1\text{Ry}}$ and $P_{2\text{Ry}}$ are treated on equal footing.

Clearly, single atom excitation $P_{1\text{Ry}}$, or pair excitation $P_{2\text{Ry}}$ at large interatomic distances R , are unaffected by the Rydberg-state interactions. Scanning the frequency of the laser field, we then probe the microwave field induced Autler-Townes doublet $\lambda_{\pm} = -\frac{1}{2}\Delta \pm \sqrt{\frac{1}{4}\Delta^2 + \Omega^2}$ of the Rydberg states $|e\rangle$ and $|r\rangle$. For large microwave detuning $|\Delta| \gg \Omega$, the probe field resonances are at $\Delta_p^{(-)} = \lambda_- \simeq -\frac{\Omega^2}{|\Delta|}$ and $\Delta_p^{(+)} = \lambda_+ \simeq |\Delta| + \frac{\Omega^2}{|\Delta|}$, as expected [cf. Fig. 1(c)]. Importantly, in the frequency region between $\Delta_p^{(-)}$ and $\Delta_p^{(+)}$, destructive quantum interference leads to a dark resonance (EIT window) for the probe pulse [40, 41]: If the pulse envelope varies adiabatically, $\partial_t\Omega_p < \Omega_p|\lambda_+ - \lambda_-|$, it does not excite the bright eigenstates of the three-level atom, which correspond to the Autler-Townes doublet when $\Omega_p \ll \Omega$. During the interaction with the pulse, the populations of the Rydberg states are $\langle\hat{\sigma}_{ee}\rangle \simeq 0$ and $\langle\hat{\sigma}_{rr}\rangle \simeq \frac{\Omega_p^2}{\Omega^2}$, but after the interaction, $\Omega_p \rightarrow 0$, the atom returns to the ground state with ideally unit probability $\langle\hat{\sigma}_{gg}\rangle \simeq 1$. Atomic coherence relaxation γ , however, reduces the transparency causing residual population of the excited states.

Hence, within the EIT window for a single (non-interacting) atom, we can probe the two-atom Rydberg

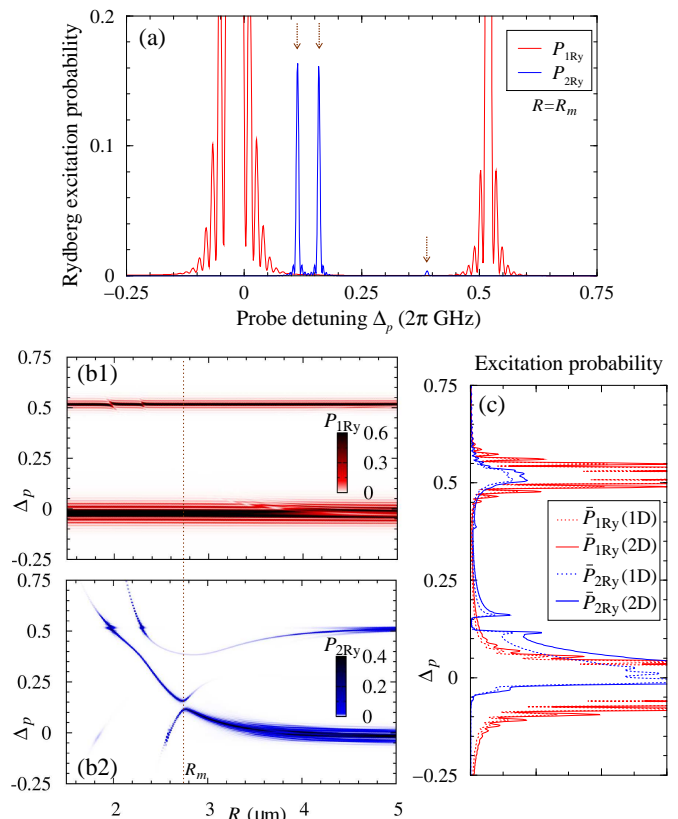


FIG. 2. Rydberg excitation spectra for two atoms excited from the ground state $|gg\rangle$ by a smooth probe pulse $\Omega_p(t)$. (a) One- and two-atom excitation probabilities $P_{1\text{Ry}}$ and $P_{2\text{Ry}}$ at interatomic distance $R = R_m = 2.74 \mu\text{m}$. (b1), (b2) Density plots of $P_{1\text{Ry}}, P_{2\text{Ry}}$ vs distance R [vertical dotted line marks $R = R_m$, cf. (a)]. (c) Spatially averaged excitation probabilities $\bar{P}_{1\text{Ry}}, \bar{P}_{2\text{Ry}}$ for pairs of atoms in a 1D or 2D volume of linear dimension $L = 5 \mu\text{m}$. In the simulations, the decay rates are $\Gamma_{e,r} = 5 \text{ kHz}$ and $\gamma_g = 2\pi \times 100 \text{ kHz}$, the probe Rabi frequency $\Omega_p = 2\pi \times 10 \text{ MHz}$ (0.1Ω) and duration $\tau_p = 80 \text{ ns}$ (flat-top pulse with Gaussian leading and trailing edges of 10 ns duration); other parameters are as in Fig. 1(c).

resonances $E_{l,m,u}$. In Fig. 2(a) we show the Rydberg excitation probabilities versus probe detuning Δ_p for the atoms at distance $R = R_m$ of the E_m potential minimum. Figure 2(b) summarizes the results of our simulations for all (relevant) probe frequencies and interatomic distances. Note that selective excitation of two-atom Rydberg resonances from the ground state, $2\Delta_p = E_{l,m,u}/\hbar$, requires two probe photons and such processes are therefore second order in Ω_p , while single-atom resonances $\Delta_p = \lambda_{\pm}$ involve only one probe photon and are linear in Ω_p . An effective probe Rabi frequency for a single-atom excitation is then much smaller than for a two-atom excitation, and in Fig. 2 the smaller peaks of $P_{2\text{Ry}}$ arise from a fractional ($\frac{1}{10}$) two-atom Rabi cycle, while the same amplitude and duration of the probe pulse results in several single-atom Rabi cycles leading to large and broad (sinc-shaped) peaks of $P_{1\text{Ry}}$.

Note that a small excitation probability of the anti-symmetric potential curve E_{er-} seen in Fig. 2(b2) (lower left corner) is due to dephasing γ of individual atomic coherences.

If two atoms are confined in a uniform 1D (line) or 2D (disc) volume of linear dimension L , we can average the Rydberg excitation probabilities over the interatomic distances, $\bar{P}_{1,2Ry} \equiv \int_0^L P_{1,2Ry} \varrho(R) dR$, where the corresponding probability densities for distances R are given by $\varrho_{1D}(R) = \frac{2(L-R)}{L^2}$ and $\varrho_{2D}(R) = \frac{8R}{\pi L^2} \left[2 \arccos \frac{R}{L} - \frac{R}{2L} \sqrt{1 - \frac{R^2}{L^2}} \right]$. As seen in Fig. 2(c), even after averaging over a large volume, we can still discern the structure of the two-atom Rydberg excitation probabilities \bar{P}_{2Ry} exhibiting an energy gap $2\Omega^{(2)} \simeq 2\pi \times 0.1 \text{GHz}$ between $\max E_l/2\hbar < \Delta_p < \min E_m/2\hbar$, not masked by the single-atom excitation probability \bar{P}_{1Ry} within the EIT window. Such features may still persist in low-density many-atom experiments, provided the probability of having three- or more atoms within a few μm distance is small compared to the two-atom probability.

We now describe a potential application of the coherent, selective excitation of the Rydberg-dimer state for quantum information processing. Assume that a pair of cold atoms 1 and 2 are trapped at a relative distance $R_0 \simeq R_m$ in an optical lattice [38, 39] or by far-detuned focused laser beams [6–8]. In each atom, long-lived states $\{|s\rangle, |g\rangle\}$ represent the qubit basis states. The probe field resonantly couples the two-atom ground state $|g_1g_2\rangle$ to the bound Rydberg-dimer state with the effective two-photon Rabi frequency $\Omega_p^{(2)} \sim f\Omega_p/\Delta_p$, where f is the Franck-Condon overlap between the corresponding relative-coordinate wavefunctions [42]. Atoms in state $|s\rangle$ are decoupled from the field, while single-atom Rydberg excitations from $|g\rangle$ are suppressed by the EIT mechanism. A pulse of effective area $\theta_p = 2 \int_0^\tau \Omega_p^{(2)}(t) dt = 2\pi$ thus leads to precisely one Rabi cycle between $|g_1g_2\rangle$ and the Rydberg-dimer state, while all other initial states remain unaltered. The resulting π phase shift of $|g_1g_2\rangle$ corresponds to the two-qubit CPHASE logic gate [43, 44].

We have performed simulations of the two-atom gate using realistic experimental parameters [42]. As seen in Fig. 3(insets), sizable dephasing γ detrimentally affects the amplitude of Rabi oscillations between the two-atom internal-motional ground state and the lowest bound Rydberg-dimer state, and causes leakage of population to the vibrationally excited Rydberg-dimer states [42], reducing thereby the final population $P_{gg} = \langle \hat{\sigma}_{gg}^1 \otimes \hat{\sigma}_{gg}^2 \rangle$ of state $|g_1g_2\rangle$. To quantify the performance of the gate, we apply it to the input state $|\Psi_{\text{in}}\rangle = \frac{1}{2}(|s_1\rangle + |g_1\rangle) \otimes (|s_2\rangle + |g_2\rangle)$ containing equally weighted superposition of all two-qubit states. Ideally, the output state should be $|\Psi_{\text{out}}\rangle = \frac{1}{2}(|s_1s_2\rangle + |s_1g_2\rangle + |g_1s_2\rangle - |g_1g_2\rangle)$. In Fig. 3 we show the resulting gate fidelity $F = \langle \Psi_{\text{out}} | \hat{\rho}(\tau) | \Psi_{\text{out}} \rangle$

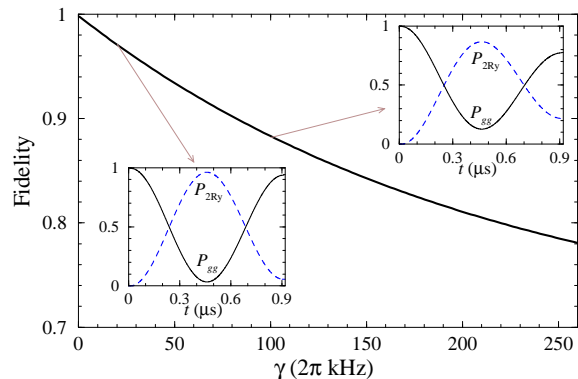


FIG. 3. Fidelity F of CPHASE gate performed on atomic qubits trapped at relative distance R_m vs dephasing rate γ . Insets show probabilities P_{gg} and P_{2Ry} of two-atom ground and bound Rydberg-dimer states during one Rabi cycle, for $\gamma/(2\pi) = 20$ and 100 kHz. Probe pulse detuning is $\Delta_p = 2\pi \times 159.3 \text{MHz}$, duration $\tau = 0.9 \mu\text{s}$ and its single-atom Rabi frequency $\sqrt{f}\Omega_p$ is scaled by the Franck-Condon factor $f = 0.65$ [42]. Other parameters are as in Fig. 2(a).

which is close to unity for small $\gamma \ll \Omega_p^{(2)}$, but decreases with increasing γ , as expected.

Our quantum logic gate implementation complements previous proposals [6] in several ways. For moderate interatomic separation of a few micrometers, the strong interactions are typically used for the blockade gate [2] involving resonant excitation of only one Rydberg atom [6–8], while at larger separation, both atoms can be excited and the interaction causes phase shift accumulated over time [2, 9]. One can attempt to excite resonantly an anti-blockaded pair of strongly interacting atoms while suppressing single-atom excitation by large detuning (equal to half the interaction energy), but then the gradient of the vdW potential amounts to strong mechanical force between the atoms, causing motional decoherence and even excitation suppression [21]. In our implementation of a fast interaction gate, single atom excitations are not merely suppressed by large detuning, but are almost completely canceled by destructive quantum interference, and the gate is much less vulnerable to motional decoherence since we resonantly excite the two-atom Rydberg state at a potential minimum.

We are grateful to I. Lesanovsky and W. Li for valuable input and discussions, and we acknowledge support from the Aarhus University Research Foundation (AUFF), the FET-Open grant MALICIA (265522) and the Villum Foundation.

-
- [1] T.F. Gallagher, *Rydberg Atoms* (Cambridge University Press, Cambridge, 1994).
 [2] D. Jaksch, J.I. Cirac, P. Zoller, S.L. Rolston, R. Cote, and M.D. Lukin, *Phys. Rev. Lett.* **85**, 2208 (2000).

- [3] M.D. Lukin, M. Fleischhauer, R. Côté, L.M. Duan, D. Jaksch, J.I. Cirac, and P. Zoller, *Phys. Rev. Lett.* **87**, 037901 (2001).
- [4] M. Saffman, T.G. Walker, and K. Mølmer, *Rev. Mod. Phys.* **82**, 2313 (2010).
- [5] D. Comparat and P. Pillet, *J. Opt. Soc. Am. B* **27**, A208 (2010).
- [6] A. Gaëtan, Y. Miroshnychenko, T. Wilk, A. Chotia, M. Viteau, D. Comparat, P. Pillet, A. Browaeys, and P. Grangier, *Nature Phys.* **5**, 115 (2009); T. Wilk, A. Gaëtan, C. Evellin, J. Wolters, Y. Miroshnychenko, P. Grangier, and A. Browaeys, *Phys. Rev. Lett.* **104**, 010502 (2010).
- [7] E. Urban, T.A. Johnson, T. Henage, L. Isenhower, D.D. Yavuz, T.G. Walker, and M. Saffman, *Nature Phys.* **5**, 110 (2009); L. Isenhower, E. Urban, X. L. Zhang, A. T. Gill, T. Henage, T. A. Johnson, T. G. Walker, and M. Saffman, *Phys. Rev. Lett.* **104**, 010503 (2010).
- [8] L. Beguin, A. Vernier, R. Chicireanu, T. Lahaye, and A. Browaeys, *Phys. Rev. Lett.* **110**, 263201 (2013).
- [9] D. D. Bhaktavatsala Rao and K. Mølmer, *Phys. Rev. A* **89**, 030301(R) (2014).
- [10] Y.O. Dudin, L. Li, F. Bariani, and A. Kuzmich, *Nature Phys.* **8**, 790 (2012); L. Li, Y.O. Dudin, and A. Kuzmich, *Nature* **498**, 466 (2013).
- [11] H. Weimer, M. Müller, I. Lesanovsky, P. Zoller, and H.P. Büchler, *Nature Phys.* **6**, 382 (2010).
- [12] C.H. Greene, A.S. Dickinson, and H.R. Sadeghpour, *Phys. Rev. Lett.* **85**, 2458 (2000).
- [13] V. Bendkowsky, B. Butscher, J. Nipper, J.P. Shaffer, R. Löw, and T. Pfau, *Nature* **458**, 1005 (2009); W. Li, T. Pohl, J.M. Rost, S.T. Rittenhouse, H.R. Sadeghpour, J. Nipper, B. Butscher, J.B. Balewski, V. Bendkowsky, R. Löw, and T. Pfau, *Science* **334**, 1110 (2011).
- [14] C. Boisseau, I. Simbotin, and R. Cote, *Phys. Rev. Lett.* **88**, 133004 (2002).
- [15] A. Schwettmann, K.R. Overstreet, J. Tallant, and J.P. Shaffer, *J. Mod. Opt.* **54**, 2551 (2007); K.R. Overstreet, A. Schwettmann, J. Tallant, D. Booth, and J.P. Shaffer, *Nature Phys.* **5**, 581 (2009).
- [16] N. Samboy, J. Stanojevic, and R. Cote, *Phys. Rev. A* **83**, 050501(R) (2011).
- [17] M. Kiffner, H. Park, W. Li, and T.F. Gallagher, *Phys. Rev. A* **86**, 031401(R) (2012).
- [18] M. Kiffner, W. Li, and D. Jaksch, *Phys. Rev. Lett.* **111**, 233003 (2013).
- [19] Y. Yu, H. Park, and T. F. Gallagher, *Phys. Rev. Lett.* **111**, 173001 (2013).
- [20] C. Ates, B. Olmos, W. Li, and I. Lesanovsky, *Phys. Rev. Lett.* **109**, 233003 (2012).
- [21] W. Li, C. Ates, and I. Lesanovsky, *Phys. Rev. Lett.* **110**, 213005 (2013).
- [22] G. Pupillo, A. Micheli, M. Boninsegni, I. Lesanovsky, and P. Zoller, *Phys. Rev. Lett.* **104**, 223002 (2010).
- [23] H. Weimer, R. Löw, T. Pfau, and H.P. Büchler, *Phys. Rev. Lett.* **101**, 250601 (2008).
- [24] H. Weimer and H.P. Büchler, *Phys. Rev. Lett.* **105**, 230403 (2010).
- [25] T. Pohl, E. Demler, and M.D. Lukin, *Phys. Rev. Lett.* **104**, 043002 (2010).
- [26] J. Schachenmayer, I. Lesanovsky, A. Micheli, and A.J. Daley, *New J. Phys.* **12**, 103044 (2010).
- [27] R.M.W. van Bijnen, S. Smit, K.A.H. van Leeuwen, E.J.D. Vredenbregt, and S.J.J.M.F. Kokkelmans, *J. Phys. B* **44**, 184008 (2011).
- [28] I. Lesanovsky, *Phys. Rev. Lett.* **106**, 025301 (2011).
- [29] I. Lesanovsky, *Phys. Rev. Lett.* **108**, 105301 (2012).
- [30] W. Zeller, M. Mayle, T. Bonato, G. Reinelt, and P. Schmelcher, *Phys. Rev. A* **85**, 063603 (2012).
- [31] S. Ji, C. Ates and I. Lesanovsky, *Phys. Rev. Lett.* **107**, 060406 (2011).
- [32] C. Ates and I. Lesanovsky, *Phys. Rev. A* **86**, 013408 (2012).
- [33] D. Petrosyan, M. Höning, and M. Fleischhauer, *Phys. Rev. A* **87**, 053414 (2013).
- [34] M. Höning, D. Muth, D. Petrosyan, and M. Fleischhauer, *Phys. Rev. A* **87**, 023401 (2013).
- [35] M. Gärttner, K.P. Heeg, T. Gasenzer and J. Evers, *Phys. Rev. A* **86**, 033422 (2012); *Phys. Rev. A* **88**, 043410 (2013).
- [36] D. Petrosyan, *J. Phys. B* **46**, 141001 (2013); *Phys. Rev. A* **88**, 043431 (2013).
- [37] I. Lesanovsky and J. P. Garrahan *Phys. Rev. Lett.* **111**, 215305 (2013).
- [38] M. Viteau, M.G. Bason, J. Radogostowicz, N. Malossi, D. Ciampini, O. Morsch, and E. Arimondo, *Phys. Rev. Lett.* **107**, 060402 (2011).
- [39] P. Schauf, M. Cheneau, M. Endres, T. Fukuhara, S. Hild, A. Omran, T. Pohl, C. Gross, S. Kuhr, and I. Bloch, *Nature* **491**, 87 (2012).
- [40] K. Bergmann, H. Theuer, and B.W. Shore, *Rev. Mod. Phys.* **70**, 1003 (1998).
- [41] M. Fleischhauer, A. Imamoglu, and J. P. Marangos, *Rev. Mod. Phys.* **77**, 633 (2005).
- [42] See Supplemental Material for atomic parameters and interactions, calculations of interatomic potential wells, potential curves for different geometries and microwave field detunings, and excitation of trapped ground state atoms to the Rydberg-dimer state.
- [43] M. Nielsen and I. Chuang, *Quantum Computation and Quantum Information*, (Cambridge University Press, Cambridge, 2000)
- [44] P. Lambropoulos and D. Petrosyan, *Fundamentals of Quantum Optics and Quantum Information*, (Springer, Berlin, 2007).

SUPPLEMENTAL MATERIAL

In these notes, we present details on the Rydberg states of the pair of atoms and their interactions, calculations of interatomic potential wells for large detuning of the microwave field as used in the main text, interatomic potentials for different geometries and microwave field detunings, and the Franck-Condon factors for coherent excitation of trapped ground state atoms to the bound Rydberg dimer states.

Atomic parameters and interatomic interactions

The vector \mathbf{R} connecting the positions of atoms 1 and 2 forms an angle θ with the quantization direction \hat{z} defined by a static electric field \mathbf{E} , see Fig. 4(a). The interaction between the atomic dipoles \wp_1 and \wp_2 is given by

$$\begin{aligned} \mathcal{D} &= \frac{1}{4\pi\epsilon_0} \left[\frac{\wp_1 \cdot \wp_2}{R^3} - 3 \frac{(\wp_1 \cdot \mathbf{R})(\wp_2 \cdot \mathbf{R})}{R^5} \right] \\ &= \frac{1}{4\pi\epsilon_0 R^3} \left[\wp_{1+}\wp_{2-} + \wp_{1-}\wp_{2+} + \wp_{1z}\wp_{2z}(1 - 3\cos^2\theta) \right. \\ &\quad \left. - \frac{3}{2}\sin^2\theta(\wp_{1+}\wp_{2+} + \wp_{1+}\wp_{2-} + \wp_{1-}\wp_{2+} + \wp_{1-}\wp_{2-}) \right. \\ &\quad \left. - \frac{3}{\sqrt{2}}\sin\theta\cos\theta(\wp_{1+}\wp_{2z} + \wp_{1-}\wp_{2z} + \wp_{1z}\wp_{2+} + \wp_{1z}\wp_{2-}) \right], \end{aligned} \quad (1)$$

where $R \equiv |\mathbf{R}|$ while $\wp_{\pm,0}$ denotes the dipole matrix element for the atomic transition changing the magnetic quantum number m_j (projection of the total angular momentum J onto \hat{z}) by $\Delta m_j = \pm 1, 0$. The interaction is invariant under rotation about the \hat{z} axis.

We assume alkali atoms. The two Rydberg states of each atom are represented by $|e\rangle \equiv |nS_{1/2}, m_j = +\frac{1}{2}\rangle$ and $|r\rangle \equiv |nP_{3/2}, m_j = +\frac{3}{2}\rangle$ with the principal quantum number n ($\gtrsim 40$), see Fig. 4(b). A σ_+ -polarized

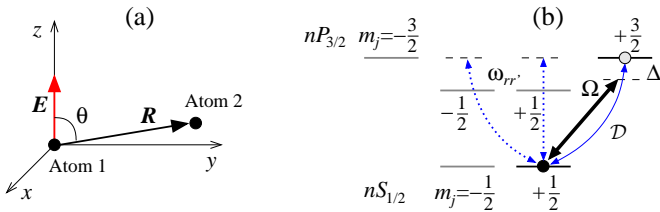


FIG. 4. (a) Geometry of the system of two Rydberg atoms: θ is the angle between the relative position vector \mathbf{R} and the quantization axis z defined by a static external field \mathbf{E} . (b) Level scheme of the magnetic sublevels m_j of states $nS_{1/2}$ and $nP_{3/2}$ of each atom. The microwave field drives the transition between $|e\rangle \equiv |nS_{1/2}, m_j = \frac{1}{2}\rangle$ and $|r\rangle \equiv |nP_{3/2}, m_j = \frac{3}{2}\rangle$ with the Rabi frequency Ω and detuning Δ . Resonant DD (exchange) interaction \mathcal{D} can swap the states $|e_1\rangle|r_2\rangle \leftrightarrow |r_1\rangle|e_2\rangle$ of the two atoms, while the transitions to $|r'_\pm\rangle \equiv |nP_{3/2}, m_j = \pm\frac{1}{2}\rangle$ are non-resonant due to the \mathbf{E} field induced differential Stark shift $\omega_{rr'}$.

microwave field \mathcal{E}_{mw} of frequency ω_{mw} drives the transition $|e\rangle \leftrightarrow |r\rangle$ with the Rabi frequency $\Omega = \wp_{er}\mathcal{E}_{\text{mw}}/\hbar$ and detuning $\Delta = \omega_{\text{mw}} - \omega_{re}$. We can recast the DD interaction as

$$\begin{aligned} \mathcal{D} &= \frac{2 - 3\sin^2\theta}{8\pi\epsilon_0 R^3} (\wp_{1+}\wp_{2-} + \wp_{1-}\wp_{2+}) \\ &\quad - \frac{3\sin^2\theta}{8\pi\epsilon_0 R^3} \left[\wp_{1+}\wp_{2+} + \wp_{1-}\wp_{2-} + \frac{\sqrt{2}\cos\theta}{\sin\theta} \right. \\ &\quad \left. \times (\wp_{1+}\wp_{2z} + \wp_{1-}\wp_{2z} + \wp_{1z}\wp_{2+} + \wp_{1z}\wp_{2-}) \right], \end{aligned} \quad (1)$$

where we neglected the term $\wp_{1z}\wp_{2z}$ since states $|r'_\pm\rangle \equiv |nP_{3/2}, m_j = \pm\frac{1}{2}\rangle$ are not populated by the microwave field. The first term on the right-hand side of Eq. (1) describes the resonant DD exchange interaction $|e_{1(2)}r_{2(1)}\rangle \leftrightarrow |r_{1(2)}e_{2(1)}\rangle$ denoted by \mathcal{D}_{eg} in the main text. The transition matrix elements are $\wp_{\pm} = \mp \frac{1}{\sqrt{3}}(nS_{1/2}||\wp||nP_{3/2})$, where the numerical prefactor corresponds the angular part while the reduced matrix element in the semiclassical approximation [1] is given by $(nS_{1/2}||\wp||nP_{3/2}) \approx -\frac{3}{2}n^{*2}$ with $n^* = n - \delta_S$ the effective principal quantum number. The DD coefficient is then $C_3^{er} \approx \frac{3(3\sin^2\theta - 2)}{32\pi\epsilon_0} n^{*4}$. The second term on the right-hand side of Eq. (1) corresponds to the DD interaction coupling states $|r_{1(2)}e_{2(1)}\rangle$ to $|e_{1(2)}r'_{2(1)}\rangle$ with rates $C_3^{re,er'} \approx \frac{3\sqrt{3}\sin^2\theta}{32\pi\epsilon_0} n^{*4}$ and $C_3^{re,er'+} \approx \frac{3\sqrt{3}\sin\theta\cos\theta}{16\pi\epsilon_0} n^{*4}$. This process could populate states $|r'\rangle$ outside the two-level subspace $\{|e\rangle, |r\rangle\}$, but we assume that this leakage is suppressed by the external electric \mathbf{E} (or magnetic) field inducing differential Stark (or Zeeman) shift $\omega_{rr'}$ between levels $|r\rangle$ and $|r'_\pm\rangle$, see Fig. 4(b). The non-resonant DD interaction induces, however, a second-order level shift of states $|r_{1(2)}e_{2(1)}\rangle$, which we account for as an effective vdW interaction $\mathcal{W}_{er} = \hbar \frac{C_6^{er}}{R^6} \hat{\sigma}_{rr}^{1(2)} \otimes \hat{\sigma}_{ee}^{2(1)}$ with the coefficient $C_6^{er} = \sum_{r'} \frac{|C_3^{re,er'}|^2}{\omega_{rr'}}$, which is positive (repulsive vdW interaction) if levels $|r'\rangle$ are lower than $|r\rangle$. We note that this is a rather simplistic approximation which, strictly speaking, is valid only at large enough distances $R > \sqrt[3]{\frac{|C_3^{re,er'}|}{\omega_{rr'}}}$. The combination of resonant and nonresonant DD interactions and the resulting binding potential was analyzed rigorously in [2], while our simplification facilitates derivation of the hitherto unexplored binding potentials originating from microwave dressing of vdW interacting states $|e_1e_2\rangle$ and $|r_1r_2\rangle$.

To be specific, we take Rb atoms in $n = 60$ states. The quantum defects for the $S_{1/2}$ and $P_{3/2}$ states are $\delta_S = 3.13109$ and $\delta_P = 2.65145$ [3], with which the (unshifted) $|e\rangle \rightarrow |r\rangle$ transition frequency is $\omega_{re} \simeq 2\pi \times 17$ GHz. In the main text, we consider the case $\theta = \frac{\pi}{2}$ when the quantization axis \hat{z} is perpendicular to the two-atom separation vector \mathbf{R} . For the DD interaction, we then obtain $C_3^{er} \approx 2\pi \times 3.8 \text{ GHz } \mu\text{m}^3$ and assume

$C_6^{er} = 2\pi \times 3 \text{ GHz } \mu\text{m}^6$, while the coefficients for the vdW potentials \mathcal{W}_{ee} and \mathcal{W}_{rr} are $C_6^{ee} \simeq 2\pi \times 140 \text{ GHz } \mu\text{m}^6$ (repulsion) and $C_6^{rr} \simeq -2\pi \times 295 \text{ GHz } \mu\text{m}^6$ (attraction) [4, 5]. For other values of θ (see below), the angular dependence of the DD and vdW coefficients is $C_3^{er}(\theta) \propto (3 \sin^2 \theta - 2)$ and $C_6^{rr}(\theta) \propto \sin^2 \theta$, while C_6^{ee} remains isotropic [4].

Crossing points of $E_{\alpha\beta}$ and potential minima of $E_{m,u}$

For vanishing microwave field amplitude, $\Omega \rightarrow 0$, the crossing points of the bare two-atom potentials E_{ee} , E_{er+} , and E_{rr} are

$$E_{ee} = E_{er+} \equiv E_{c1} = \frac{4\hbar\Delta^2 C_6^{ee}}{\left[\sqrt{(C_3^{er})^2 + 4|\Delta|(C_6^{ee} - C_6^{er}) - C_3^{er}}\right]^2}$$

$$\text{at } R_1 = \left[\sqrt{\left(\frac{C_3^{er}}{2\Delta}\right)^2 + \frac{C_6^{ee} - C_6^{er}}{|\Delta|} - \frac{C_3^{er}}{2|\Delta|}} \right]^{1/3},$$

$$E_{rr} = E_{er+} \equiv E_{c3} = -2\hbar\Delta + \frac{4\hbar\Delta^2 C_6^{rr}}{\left[\sqrt{(C_3^{er})^2 + 4|\Delta|(C_6^{er} - C_6^{rr}) + C_3^{er}}\right]^2}$$

$$\text{at } R_3 = \left[\sqrt{\left(\frac{C_3^{er}}{2\Delta}\right)^2 + \frac{C_6^{er} - C_6^{rr}}{|\Delta|} + \frac{C_3^{er}}{2|\Delta|}} \right]^{1/3},$$

and

$$E_{ee} = E_{rr} \equiv E_{c2} = \frac{2\hbar|\Delta|C_6^{ee}}{C_6^{ee} - C_6^{rr}} \text{ at } R_2 = \sqrt[6]{\frac{C_6^{ee} - C_6^{rr}}{2|\Delta|}}.$$

With the atomic parameters listed above, we have $R_1 \simeq 2.36 \mu\text{m}$, $R_2 \simeq 2.75 \mu\text{m}$, and $R_3 \simeq 3.05 \mu\text{m}$.

In Fig. 1(c) of the main text, the potential energy curves E_m and E_u have potential minima. Consider first the potential well on the E_m curve which is defined by the bare energy levels E_{ee} and E_{rr} crossing at R_2 . The microwave field couples states $|ee\rangle$ and $|rr\rangle$ by a two-photon transition via non-resonant intermediate state $|er+\rangle$ with the effective Rabi frequency $\Omega^{(2)} = \frac{\hbar|\sqrt{2}\Omega|^2}{E_{c2} - E_{er+}}$.

At R_2 , we have $E_{er+} \approx \hbar|\Delta| + \frac{\hbar C_3^{er} \sqrt{2|\Delta|}}{\sqrt{C_6^{ee} - C_6^{rr}}}$, which upon substitution leads to

$$\Omega^{(2)} = \frac{2|\Omega|^2(C_6^{ee} - C_6^{rr})}{|\Delta|(C_6^{ee} + C_6^{rr}) - C_3^{er} \sqrt{2\Delta(C_6^{ee} - C_6^{rr})}}.$$

For our parameters, both terms in the denominator are comparable and hence the DD interaction cannot be neglected. We obtain $|\Omega^{(2)}| \simeq 2\pi \times 55 \text{ MHz}$.

In the vicinity of E_{c2} and R_2 , we thus have an effective two-level system described by Hamiltonian

$$\mathcal{H}_{\text{eff}} = \begin{bmatrix} E_{ee}^{(1)} & \hbar\Omega^{(2)} \\ \hbar\Omega^{(2)} & E_{rr}^{(1)} \end{bmatrix},$$

where $E_{\alpha\alpha}^{(1)} = E_{c2} + \eta_{\alpha\alpha}(R - R_2)$ are linear approximations for the bare energies of the corresponding states

($\alpha\alpha = ee, rr$), with $\eta_{\alpha\alpha} = \frac{\partial E_{\alpha\alpha}}{\partial R} \Big|_{R_2}$. The binding potential is $E_m = \frac{1}{2}[E_{ee}^{(1)} + E_{rr}^{(1)}] + \sqrt{\frac{1}{4}[E_{ee}^{(1)} - E_{rr}^{(1)}]^2 + |\hbar\Omega^{(2)}|^2}$, whose minimum R_m is found by $\partial_R E_m = 0$. Expanding E_m up to the second order in R around R_m , we obtain the harmonic potential $E_m \approx (E_{c2} + \hbar\Omega^{(2)}) + \frac{1}{2}\kappa_m(R - R_m)^2$ with

$$\kappa_m = \frac{2}{\hbar|\Omega^{(2)}|} \frac{|\eta_{ee}\eta_{rr}|^{3/2}}{|\eta_{ee}| + |\eta_{rr}|} = \frac{2\hbar(12\Delta)^2(C_6^{ee}|C_6^{rr}|)^{3/2}}{R_2^2|\Omega^{(2)}|(C_6^{ee} + |C_6^{rr}|)^3}.$$

Since $\kappa_m = \mu\nu_m^2$, with μ the reduced mass, the relative vibration frequency of two identical atoms of mass M_{at} is $\nu_m \approx \sqrt{2\kappa_m/M_{\text{at}}}$. With the parameters for ^{87}Rb atoms listed above, we have $\nu_m \simeq 2\pi \times 2 \text{ MHz}$ around $R_m = 2.74 \mu\text{m}$.

Since the depth of the binding potential $\sim |\Delta|$ is much larger than the vibrational frequency ν_m , the harmonic approximation holds for many vibrational states $n \ll |\Delta|/\nu_m \sim 10^2$ of the Rydberg dimer, whose energies are given by $\varepsilon_n \simeq \hbar\nu_m(\frac{1}{2} + n)$ while the corresponding wavefunctions are

$$\chi_m(R, n) = \frac{2^{-n/2}}{\sqrt{n!}} \left(\frac{1}{\pi\Sigma_m^2}\right)^{1/4} e^{-\frac{(R-R_m)^2}{2\Sigma_m^2}} H_n\left(\frac{R}{\sqrt{\pi}\Sigma_m}\right), \quad (2)$$

where $\Sigma_m = \sqrt{2\hbar/M_{\text{at}}\nu_m}$ and $H_n(R)$ are the Hermite polynomials.

Consider now the E_u potential energy curve. The potential well is bounded by E_{ee} on the left and E_{rr} on the right sides, and E_{er+} at the bottom. Since with increasing distance R the DD interaction slowly lowers E_{er+} while E_{rr} rapidly approaches $2|\Delta|$, the minimum of the potential well is located above, and to the left from, the energy level crossing point E_{c3} , R_3 of the bare states $|er+\rangle$ and $|rr\rangle$ coupled by the microwave field with the Rabi frequency $\sqrt{2}\Omega$. Now the Hamiltonian for the effective two-level system is

$$\mathcal{H}_{\text{eff}} = \begin{bmatrix} E_{er+}^{(1)} & \hbar\sqrt{2}\Omega \\ \hbar\sqrt{2}\Omega & E_{rr}^{(1)} \end{bmatrix},$$

where $E_{\alpha\beta}^{(1)} = E_{c3} + \eta_{\alpha\beta}(R - R_3)$ with $\eta_{\alpha\beta} = \frac{\partial E_{\alpha\beta}}{\partial R} \Big|_{R_3}$. Proceeding as above, we obtain for the potential well $E_u \approx (E_{c3} + \hbar\sqrt{2}\Omega) + \frac{1}{2}\kappa_u(R - R_u)^2$ with

$$\kappa_u = \frac{2}{\hbar\sqrt{2}|\Omega|} \frac{|\eta_{er+}\eta_{rr}|^{3/2}}{|\eta_{er+}| + |\eta_{rr}|} \simeq \frac{2\hbar9|\Delta|^{5/4}(C_3^{er})^{3/2}}{R_3^2|\Omega||C_6^{rr}|^{3/4}},$$

where we assumed $R_3 \simeq \sqrt[6]{|C_6^{rr}/\Delta|}$ and neglected $C_3^{er}R_3^3$ in comparison with $2|C_6^{rr}|$ since the DD interaction varies slowly compared to the vdW interaction. For the vibration frequency of the two-atom relative motion around $R_u = 2.85 \mu\text{m}$, we then obtain $\nu_u \approx 2\pi \times 450 \text{ kHz}$.

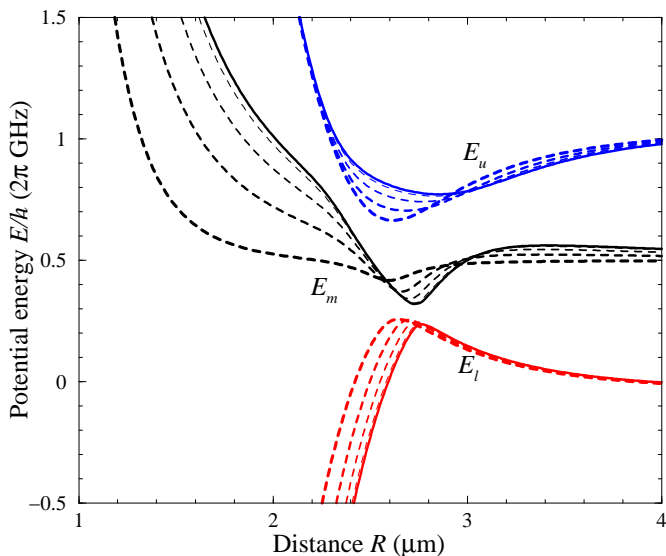


FIG. 5. Potential curves $E_{l,m,u}$ for the two-atom microwave-dressed Rydberg states, for the same parameters as in the main text but different θ : Solid curves are for $\theta = \frac{\pi}{2}$ [as in Fig. 1(c)], with the increment of $\delta\theta = 0.05\pi$ for progressively thicker dashed curves, up to $\theta = 0.7\pi$.

Two-atom potentials for $\theta \neq \frac{\pi}{2}$

In the main text, we consider the case of $\theta = \frac{\pi}{2}$ corresponding to the quantization axis \hat{z} being perpendicular to the two-atom separation vector \mathbf{R} (cf. Fig. 4 above). In Fig. 5 we show the potential curves $E_{l,m,u}$ for values of $\theta \neq \frac{\pi}{2}$. As seen, small variations of angle θ around $\frac{\pi}{2}$ change the interatomic potentials only little. With increasing $|\theta - \frac{\pi}{2}|$, the broad potential well on the upper curve E_u becomes deeper and moves towards smaller distances R . Simultaneously, the potential well on the middle curve E_m gets shallower until it nearly disappears for $\theta \gtrsim 0.7\pi$ when the strength of the attractive potential $C_6^{rr}(\theta) \propto \sin^2\theta$ becomes comparable to, or smaller than, that of the repulsive potential C_6^{ee} , which does not depend on θ .

The interatomic potentials are azimuthally symmetric, i.e., the potential curves $E_{l,m,u}$ are invariant under rotation of the interatomic separation vector \mathbf{R} about the \hat{z} axis, which would draw 2D doughnut shaped potential surfaces.

Two-atom potentials for near-resonant microwave field

In the main text, we considered the case of a large negative detuning $\Delta < -|\Omega|$ of the microwave field from the single-atom transition resonance $|e\rangle \rightarrow |r\rangle$, which leads to two binding potentials with the depths $\sim |\Delta|$. Here we outline the (near-) resonant case $|\Delta| \lesssim |\Omega|$.

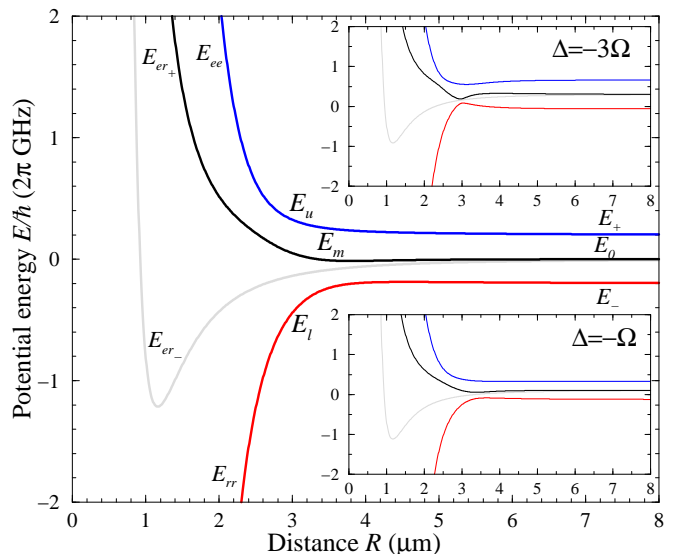


FIG. 6. Potential curves $E_{l,m,u}$ for the same parameters as in Fig. 1(c) of the main text, but with $\Delta = 0$ (main panel), and $\Delta = -\Omega$ (lower inset) and $\Delta = -3\Omega$ (upper inset).

In Fig. 6 (main panel) we show the potential energy curves for $\Delta = 0$ and $\Omega \neq 0$. Consider again the bare two-atom states $|ee\rangle$, $|er_{\pm}\rangle$, and $|rr\rangle$. The antisymmetric state $|er_{-}\rangle$ is decoupled from the field at any relative distance R , so its behavior is the same for any Δ which simply shifts the zero-point energy. At large distances $R > R_b \simeq \sqrt[6]{C_6^{\alpha\beta}/\Omega}$, $\sqrt[3]{C_3^{er}/\Omega}$, all two-atom states $|\alpha\beta\rangle$ have the same energy $E_{\alpha\beta} = 0$ (in the frame rotating with the microwave frequency). The microwave field couples resonantly the transitions $|ee\rangle \leftrightarrow |er_{+}\rangle$ and $|er_{+}\rangle \leftrightarrow |rr\rangle$ with the same Rabi frequency $\sqrt{2}\Omega$. The eigenstates of the system are then $|\Psi_0\rangle = \frac{1}{\sqrt{2}}(|ee\rangle - |rr\rangle)$ and $|\Psi_{\pm}\rangle = \frac{1}{2}(|ee\rangle \pm |er_{+}\rangle + |rr\rangle)$ with the corresponding energies $E_0 = 0$ and $E_{\pm}/\hbar = \pm\Omega$, as can be observed in Fig. 6. At small distances $R < R_b$, the vdW (and DD) shifted states $|ee\rangle$ and $|rr\rangle$ (and $|er_{+}\rangle$) are completely decoupled from the microwave field. The transition between the two regimes in the vicinity of $R = R_b$. If the attractive vdW interaction is stronger than the repulsive one, $|C_6^{rr}| > C_6^{ee}$, there is a shallow potential well on the middle curve E_m (in the opposite case of $|C_6^{rr}| < C_6^{ee}$ there would be a small hump).

With lowering the frequency of the microwave field to increase the absolute (but negative) value of the detuning $\Delta \sim -|\Omega|$, the potential well on the E_m curve becomes more pronounced [Fig. 6 lower inset]; for still larger (negative) values of $\Delta \lesssim -\Omega$, the potential energy curves approach those described in the main text [compare Fig. 6 upper inset with Fig. 1(c) of the main text].

There are no potential wells for positive detuning $\Delta > 0$, if $C_6^{rr} < 0$ and $C_6^{ee} > 0$. The situation would be reverse for repulsive vdW interaction between the upper Rydberg

states $C_6^{rr} > 0$ and attractive interaction between the lower states $C_6^{ee} < 0$, i.e., we would need $\Delta > 0$ to obtain binding potentials.

Excitation of trapped ground state atoms to the Rydberg-dimer state

We assume that the atoms $j = 1, 2$ in the ground internal state $|g\rangle$ are localized around positions $r_{j,0}$ of two separate traps. For cold atoms, we can approximate the spatial wavefunctions of the atoms ψ_j by the ground-state wavefunction of a harmonic oscillator

$$\psi_j(r_j) \approx \left(\frac{1}{\pi\sigma^2}\right)^{\frac{1}{4}} e^{-\frac{(r_j - r_{j,0})^2}{2\sigma^2}},$$

where the width $\sigma = \sqrt{\hbar/M_{\text{at}}\nu}$ is expressed through the vibrational frequency ν assumed to be the same for both atoms. The two-atom wavefunction $\Psi_{12} = \psi_1\psi_2$ can be expressed in terms of the center of mass $\bar{r} = \frac{1}{2}(r_1 + r_2)$ and relative $R = r_2 - r_1$ coordinates as $\Psi_{12}(\bar{r}, R) = \phi(\bar{r})\chi(R)$ with

$$\phi(\bar{r}) = \left(\frac{1}{\pi\bar{\sigma}^2}\right)^{\frac{1}{4}} e^{-\frac{(\bar{r} - \bar{r}_0)^2}{2\bar{\sigma}^2}}, \quad (3)$$

$$\chi(R) = \left(\frac{1}{\pi\Sigma^2}\right)^{\frac{1}{4}} e^{-\frac{(R - R_0)^2}{2\Sigma^2}}, \quad (4)$$

where $\bar{r}_0 = \frac{1}{2}(r_{1,0} + r_{2,0})$ and $R_0 = r_{2,0} - r_{1,0}$, while $\bar{\sigma} = \frac{1}{\sqrt{2}}\sigma$ and $\Sigma = \sqrt{2}\sigma$.

Our aim is to coherently and reversibly excite the two ground state atoms to a single Rydberg-dimer state on the E_m potential energy curve. We therefore assume an appropriate distance between the trapped atoms $R_0 \simeq R_m$ and apply the probe field Ω_p which is two-photon resonant between the internal-motional ground state $|G\rangle = |g_1g_2\rangle \otimes \chi(R)$ and the lowest Rydberg-dimer state $|D_m\rangle = |\Psi_m\rangle \otimes \chi_m(R)$ with

$$\chi_m(R) \equiv \chi_m(R, 0) = \left(\frac{1}{\pi\Sigma_m^2}\right)^{\frac{1}{4}} e^{-\frac{(R - R_m)^2}{2\Sigma_m^2}}, \quad (5)$$

where $\Sigma_m = \sqrt{2\hbar/M_{\text{at}}\nu_m}$. The corresponding Franck-Condon factor for the transition $|G\rangle \rightarrow |D_m\rangle$ is

$$f = \int_0^\infty \chi^*(R)\chi_m(R) dR = \left(\frac{2\Sigma\Sigma_m}{\Sigma^2 + \Sigma_m^2}\right)^{\frac{1}{2}} e^{-\frac{(R_0 - R_m)^2}{2(\Sigma^2 + \Sigma_m^2)}},$$

where we included the contribution of a possible mismatch between the equilibrium interatomic distance R_0 in the ground state traps and the position R_m of the two-atom potential minimum in the Rydberg state. Taking the trap frequency $\nu \simeq 2\pi \times 100$ kHz for the ground-state ^{87}Rb atoms, while for the Rydberg-dimer state we have $\nu_m \simeq 2\pi \times 2$ MHz (see above), we obtain

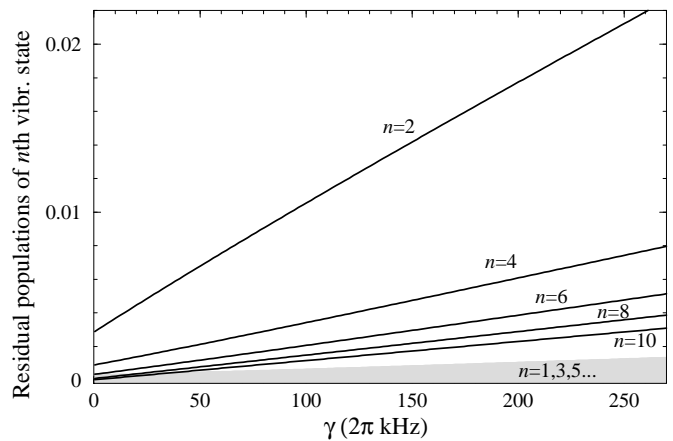


FIG. 7. Residual populations of the $n \geq 1$ vibrationally excited states of the Rydberg dimer after the effective 2π pulse implementing the CPHASE gate of Fig. 3 of the main text. The solid lines show the populations of the even- n states vs the dephasing rate γ , while the shaded area indicates the maximal possible population of the odd- n states for $|R_0 - R_m| \lesssim 0.1\Sigma_m$ mismatch of the trapping distance of the atom pair.

$\Sigma \simeq 48$ nm and $\Sigma_m \simeq 10.7$ nm. Assuming small mismatch $|R_0 - R_m| \ll \Sigma_m$ leads to the Franck-Condon factor $f \simeq 0.65$ used in Fig. 3 of the main text.

Under the harmonic approximation for the E_m binding potential, the Franck-Condon factors for the transitions between the internal-motional ground state $|G\rangle$ of a pair of atoms and n th vibrationally excited state $|D_m^{(n)}\rangle = |\Psi_m\rangle \otimes \chi_m(R, n)$ of the Rydberg dimer are given by $f(n) = \int_0^\infty \chi^*(R)\chi_m(R, n) dR$. With the above parameters and $|R_0 - R_m| = 0$, we obtain for the even excited states $f(2, 4, 6, 8, 10, \dots) = \{0.417, 0.327, 0.27, 0.229, 0.197, \dots\}$, while for all the odd excited states the Franck-Condon factors vanish, $f(1, 3, \dots) = 0$. A mismatch between R_0 and R_m , however, can make the transitions to the odd- n states allowed: e.g., for $|R_0 - R_m| \simeq 1$ nm we obtain $f(1, 3, \dots) \simeq 0.045$.

When the probe field with the effective two-photon Rabi frequency $\Omega_p^{(2)} \sim f(n)\Omega_p^2/\Delta_p$ resonantly couples the pair of ground state atoms to the lowest Rydberg-dimer state ($n = 0$), as in Fig. 3 of the main text, the vibrationally excited states $n \geq 1$ are detuned by $n\nu_m$, which, together with the smaller Franck-Condon factors $f(n)$, suppresses their excitation. In Fig. 7 above, we show the residual excitation probabilities of $n \geq 1$ vibrational states at the end of the effective $\theta_p = 2\pi$ pulse implementing the CPHASE gate. Due the small linewidths of the two-photon transitions to the Rydberg-dimer states, the populations of the even- n states are below 1% for $\gamma/(2\pi) < 100$ kHz, while the excitation probability of the closest $n = 1$ state due to a possible $|R_0 - R_m| \lesssim 1$ nm uncertainty in trap distance of the ground state atoms is less than 6.5×10^{-4} ; higher odd- n state can acquire even

less population. Hence, during the gate execution the leakage of population out of the qubit subspace into vibrationally excited Rydberg dimer states is insignificant for moderate values of dephasing γ .

We finally note that during the gate operation the center-of-mass and spatial orientation of the Rydberg dimer can disperse freely, resulting in motional decoherence. An additional weak trapping potential for the Rydberg state atoms [6] can compensate this dispersion insuring complete return of the wavefunction of the two atoms to the trapped ground state.

- [2] M. Kiffner, H. Park, W. Li, and T.F. Gallagher, Phys. Rev. A **86**, 031401(R) (2012).
- [3] T.F. Gallagher, *Rydberg Atoms* (Cambridge University Press, Cambridge, 1994).
- [4] A. Reinhard, T. Cubel Liebisch, B. Knuffman, and G. Raithel, Phys. Rev. A **75**, 032712 (2007).
- [5] K. Singer, J. Stanojevic, M. Weidemüller, and R. Côté, J. Phys. B **38**, S295 (2005).
- [6] M. Saffman, T.G. Walker, and K. Mølmer, Rev. Mod. Phys. **82**, 2313 (2010).

[1] B. Kaulakys, J. Phys. B **28**, 4963 (1995).